J Nanopart Res (2019) 21: 216
https://doi.org/10.1007/s11051-019-4662-7

RESEARCH PAPER

Surface coating–modulated peroxidase-like activity of maghemite nanoparticles for a chromogenic analysis of cholesterol

Xueqin Wang · Fan Ouyang · Liuqing Cui · Tiandi Xiong · Xinglei Guan · Yuqi Guo · Shaofeng Duan

Received: 12 June 2019 / Accepted: 9 September 2019 / Published online: 17 October 2019

Abstract Maghemite (γ-Fe_2O_3) nanoparticles (NPs) emerging as an artificial enzymes have demonstrated an excellent peroxidase-like activity and thus gained much attention in various biological and medical applications. But naked γ-Fe_2O_3 NPs are aqueously instable and prone to aggregation in biological solutions such as blood plasma. Surface coating for γ-Fe_2O_3 NPs is thus necessitated to achieve better stability and biocompatibility. In this work, three typical coating layers including poly(lactic-co-glycolic acid) (PLGA), carboxymethyl chitosan (CMCS), and human serum albumin (HSA) were utilized as modifiers to decorate γ-Fe_2O_3 NPs and fabricate compound NPs including NP_{PLGA}, NP_{CMCS}, and NP_{HSA}, respectively, and subsequently, the peroxidase-like activity of these NPs was evaluated with colorimetric analysis of cholesterol detection. The results showed that the surface coating barely affected peroxidase-like activity of NPs but could remarkably amend stability in the determined pH and temperature ranges. As evidenced with kinetic parameters, the enzymatic catalysis of NPs accorded well with Michaelis–Menten kinetics. Moreover, the catalytic assay demonstrated that the fabricated NP_{PLGA}, NP_{CMCS}, and NP_{HSA} showed a capable catalytic activity using cholesterol as substrate, and especially, the NP_{PLGA} showed a higher peroxidase-like activity compared with the NP_{CMCS} and NP_{HSA}. In conclusion, herein we obtained a coating layer-modulated peroxidase-like activity of γ-Fe_2O_3 NPs for a visualized analysis of cholesterol, which could be extended for cholesterol detection in biomedical analyses in the future.

Keywords Maghemite nanoparticles · Surface coating · Peroxidase-like activity · Cholesterol detection · Poly(lactic-co-glycolic acid) (PLGA) · Carboxymethyl chitosan (CMCS) · Human serum albumin (HSA)

Electronic supplementary material The online version of this article (https://doi.org/10.1007/s11051-019-4662-7) contains supplementary material, which is available to authorized users.

X. Wang · Y. Guo
Henan Provincial People's Hospital, School of Clinical Medicine, Henan University, Zhengzhou 450003 Henan, People's Republic of China

X. Wang · F. Ouyang · L. Cui · T. Xiong · X. Guan
College of Bioengineering, Henan University of Technology, Zhengzhou 450001 Henan, People's Republic of China

Y. Guo (✉)
International Joint Laboratory for Gynecological Oncology Nanomedicine, Zhengzhou 450003 Henan, People's Republic of China
e-mail: yuqi-guo@163.com

S. Duan (✉)
School of Pharmacy, Henan University, Kaifeng 475004 Henan, People's Republic of China
e-mail: sduan@henu.edu.cn

Introduction

Magnetic iron oxide nanoparticles (IONPs), mostly magnetite (Fe_3O_4) and maghemite (γ-Fe_2O_3), have been widely used in biomedical applications including

magnetic targeting and gene/drug delivery (Mahmoudi et al. 2009; Alexiou et al. 2000; Kurczewska et al. 2018), tumor therapy (Chung et al. 2011; Zhu et al. 2017), magnetic resonance imaging (Soares et al. 2016; Hemalatha et al. 2018), cell labeling and tracking (Olsvik et al. 1994; Gupta and Curtis 2004; Deda et al. 2017), bio-isolation and analysis (Min et al. 2012; Pérez et al. 2015), and magnetic hyperthermia (Ebrahimisadr et al. 2018; Kalidasan et al. 2016). Recently, IONPs, found with an artificial peroxidase activity, have attracted enormous interest due to their roles in biomedical diagnostics and therapeutics (Liang et al. 2013; Yang et al. 2017; Cormode et al. 2017; Gao et al. 2017). However, Fe_3O_4 NP ferrous ions may raise the toxic risk in biomedical applications (Chen et al. 2012), and thus, the oxidized γ-Fe_2O_3 NPs could be a superior candidate for a long-term bioassay.

Compared with naturally occurring peroxidase enzymes, IONPs are generally used as an artificial peroxidase with low cost and high chemical stability (Wang et al. 2017). IONPs possess an almost unchanged catalytic activity over a wide range of temperature and pH, and can be easily synthesized and purified (Lin et al. 2014). With these properties, IONPs have more applications, such as biosensing and detection (Hasanzadeh et al. 2013), immunoassays (Chen et al. 2018; Peterson et al. 2015), antibacterial agents (Situ and Samia 2014), and cancer diagnostics and therapy (Guimaraes et al. 2018; Zhu et al. 2017). However, the naked IONPs without surface coating or modification are erratic and can readily aggregate and precipitate in aqueous solutions and blood plasma, which seriously hinders their applications either as artificial enzymes in vitro or in vivo (Wang et al. 2018). To provide IONPs with such characteristics including better water-solubility, stability, low cytotoxicity, and excellent biocompatibility, extensive efforts were devoted to fabricate nanoparticles with coating layers, such as polymers (Ishihara et al. 2010), dendrimers (Boni et al. 2013), albumins (Chen et al. 2015; Kim et al. 2017), and polysaccharides (Bertholon et al. 2006; Wan et al. 2017).

Surface coating may have effects on peroxidase-like activity of Fe_3O_4 NPs in biomedical applications (Liu and Yu 2011). For instance, the polyethylene glycol (PEG) coating of Fe_3O_4 NPs resulted in a decrease in intrinsic peroxidase-like activity and led to a change in activity (Vallabani et al. 2017). However, compared with Fe_3O_4 NPs, limited information is available about the coating effects on peroxidase-like activity of γ-Fe_2O_3 NPs as peroxidase mimics.

In this work, γ-Fe_2O_3 NPs were coated with three typical molecules including poly(lactic-co-glycolic acid) (PLGA), carboxymethyl chitosan (CMCS), and human serum albumin (HSA) to fabricate complex γ-Fe_2O_3 NPs, i.e., NP_{PLGA}, NP_{CMCS}, NP_{HSA}, and then, the peroxidase-like activity of these fabricated NPs was investigated using cholesterol as a substrate via a chromogenic reaction of 3,3′,5,5′-tetramethylbenzidine (TMB) through reduction of hydrogen peroxide (H_2O_2) to H_2O. In general, in the present work, we attempted to develop a surface-modified γ-Fe_2O_3 NP with modulated catalytic activity more suitable for biomedical applications in the future.

Experimental section

Materials

Superparamagnetic γ-Fe_2O_3 NPs utilized in this study were prepared from magnetite (Fe_3O_4) according to methods proposed elsewhere (Qu et al. 1999; Sun et al. 2004). HSA, PLGA (M_W = 7000–17,000), CMCS, 3,3′,5,5′-tetramethylbenzidine (TMB), hydrogen peroxide(H_2O_2), sodium tripolyphosphate (TPP), and Triton X-100 were purchased from Sigma-Aldrich (St. Louis, MO, USA). Cholesterol, cholesterol oxidase (CHOx, 1KU) and cholesterol esterase (1KU) were purchased from Aladdin Industrial Corporation (Shanghai, China). Peroxidase (POD, ≥ 250 U/mg), glucose, glycerin, and phenol were obtained from Sinopharm Chemical Reagent Co., Ltd. (Shanghai, China). Other reagents and chemicals were purchased from local commercial suppliers and were of analytical reagent grade, unless otherwise stated. Deionized (DI) water (Milli-Q, Millipore, Bedford, MA) was used to prepare aqueous solutions.

Preparation of γ-Fe_2O_3 NPs and PLGA, CMCS, and HSA modification

In the present study, the magnetic γ-Fe_2O_3 NPs were firstly synthesized as superparamagnetic core nanocarriers through chemical co-precipitation method as previously described (Qu et al. 1999; Sun et al. 2004), and more information about synthesis of γ-Fe_2O_3 NPs are provided in the Supplementary Information (SI).

The solvent evaporation method was used to prepare the PLGA-modified magnetic nanoparticles (NP_{PLGA}) as previously described elsewhere (Varshosaz and Soheili

2008; Zhao et al. 2013). In brief, 100 mg PLGA was dissolved in 2 mL dichloromethane and added with 30 mg γ-Fe_2O_3 NPs to obtain an organic dispersion, which was subsequently poured into 20 mL 3% polyvinyl alcohol (PVA) solution to form a stable emulsion by a constant sonication. The formed NP_{PLGA} were firstly washed three times under magnetic field using DI water, then lyophilized, and stored at 4 °C until use.

The CMCS-modified magnetic nanoparticles (NP_{CMCS}) were synthesized through TPP cross-linking. Briefly, 50 mL of TPP (1 mg/mL) was mixed with γ-Fe_2O_3 (10 mg/mL) and vigorously stirred for 30 min at 60 °C. The mixture was kept for 12 h at room temperature (RT) and washed three times with DI water to obtain TPP@γ-Fe_2O_3. Ten milliliters of CMCS solution (1 % w/v, dissolved in acetic acid) was added into the TPP@γ-Fe_2O_3 and allowed to react for 30 min in ultrasonic emulsifier. The prepared NP_{CMCS} were washed three times with DI water and stored at 4 °C for further use.

The preparation of magnetic HSA-modified nanoparticles (NP_{HSA}) was followed with previously reported protocol with minor modifications (Wang et al. 2009). More information was provided in the Supplementary information (SI).

Stability analysis of the prepared NP_{PLGA}, NP_{CMCS}, and NP_{HSA}

The stability of the prepared NP_{PLGA}, NP_{CMCS}, and NP_{HSA} in DI water was analyzed according to a previously described protocol (Wang et al. 2009). The composites including NP_{PLGA}, NP_{CMCS}, and NP_{HSA} (100 μg/mL) were ultrasonically dispersed in DI water at RT. Subsequently, the stability of various composites was detected by measuring the optical absorbance of the dispersions at predetermined time points at 480 nm by using a UV-Vis spectrophotometer.

Measurement of peroxidase-like activity of the composites

The peroxidase-like activity of the prepared NP_{PLGA}, NP_{CMCS}, and NP_{HSA} was investigated in 1.5-mL tubes with the concentration ranging from 5 to 200 μg/mL. Then, 25 ng POD was used as a positive control in 200 μL reaction buffer (0.2 M NaAc, pH 3.6) in the presence of 12.8 μL of H_2O_2 (30%) for γ-Fe_2O_3 NPs, NP_{PLGA}, NP_{CMCS}, and NP_{HSA}. Afterwards, 0.2 μL of 100 μM TMB was added as the substrate. Color reactions were immediately observed. After incubation at 37 °C for 15 min in the dark, photographs were taken and the supernatant was measured by the UV-Vis spectrophotometer and the maximal absorbance of oxidized TMB (oxTMB) was recorded at 652 nm 6 h later; the reactions were stopped by adding 50 μL of 0.5 M sulfuric acid (H_2SO_4).

To analyze the reaction kinetics, steady-state kinetics assays of NP_{PLGA}, NP_{CMCS}, and NP_{HSA} (50 μg/mL) toward TMB oxidation were carried out with varied concentrations of the substrate TMB or H_2O_2 at 37 °C. The absorbance of the reaction solution was monitored in time-scan mode at 652 nm (Josephy et al. 1982). The kinetic parameters of the catalytic reaction were determined on the basis of the Lineweaver–Burk plots of the double reciprocal of the Michaelis–Menten equation:

$$\frac{1}{\nu} = \frac{K_m}{V_m}\left(\frac{1}{[S]} + \frac{1}{K_m}\right)$$

where v is the initial velocity of the reaction, V_{max} is the maximal rate of reaction, [S] is the substrate concentration, and K_m is the Michaelis−Menten constant, which is equivalent to the substrate concentration at which the rate of conversion is half of V_{max} and denotes the affinity of the enzyme (Dong et al. 2012). V_{max} was calculated into molar change from UV absorbance on the basis of the equation of $A = \varepsilon lc$ (where A is the absorbance, ε is the absorbance coefficient, l is the path length, and c is the molar concentration) with $\varepsilon = 3.9 \times 10^4$ $M^{-1}cm^{-1}$ and l = 10 mm (Singh 2016).

In addition, 0.2 M NaAc (pH 3.0–5.5) was used to study the influence of reaction buffer pH on the relative activity of the prepared NP_{PLGA}, NP_{CMCS}, and NP_{HSA}, and the varying incubation temperature (from 30 to 55 °C) was also examined to reveal the influence on the relative catalytic activity of the prepared nanoparticles under identical conditions.

Colorimetric analysis of cholesterol

Cholesterol detection was performed as follows: (i) 10 μL of CHOx (100 UN/mL) was mixed with 100 μL of cholesterol with different concentrations in Triton X-100 solution (0.3%) and added with 90 μL PBS buffer (0.5 mM, pH 7.0), followed by incubation at 37 °C for 30 min. (ii) 1.96 μL of 0.6 mM TMB; 100 μL of γ-Fe_2O_3, together with NP_{PLGA}, NP_{CMCS}, or NP_{HSA} (250 μg/mL); and 200 μL of NaAc (0.2 M, pH 3.6) were

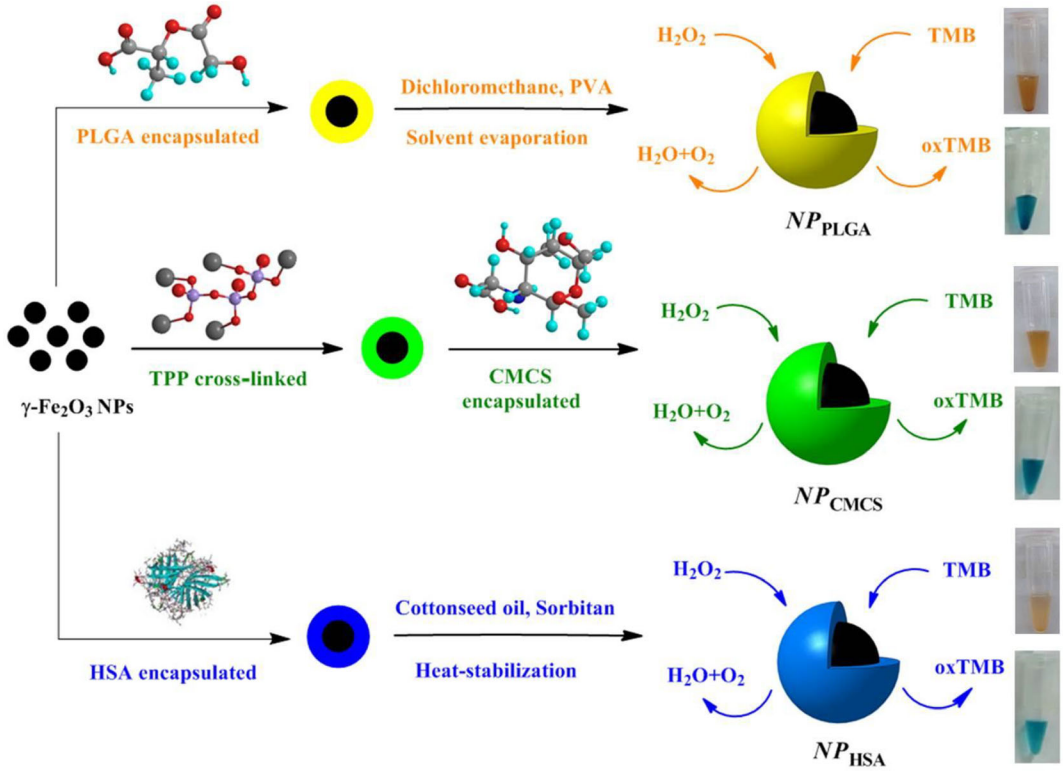

Scheme 1 Schematic illustration for catalysis detection of the peroxidase-like activity of NP_{PLGA}, NP_{CMCS}, and NP_{HSA} in the TMB–H_2O_2 system.

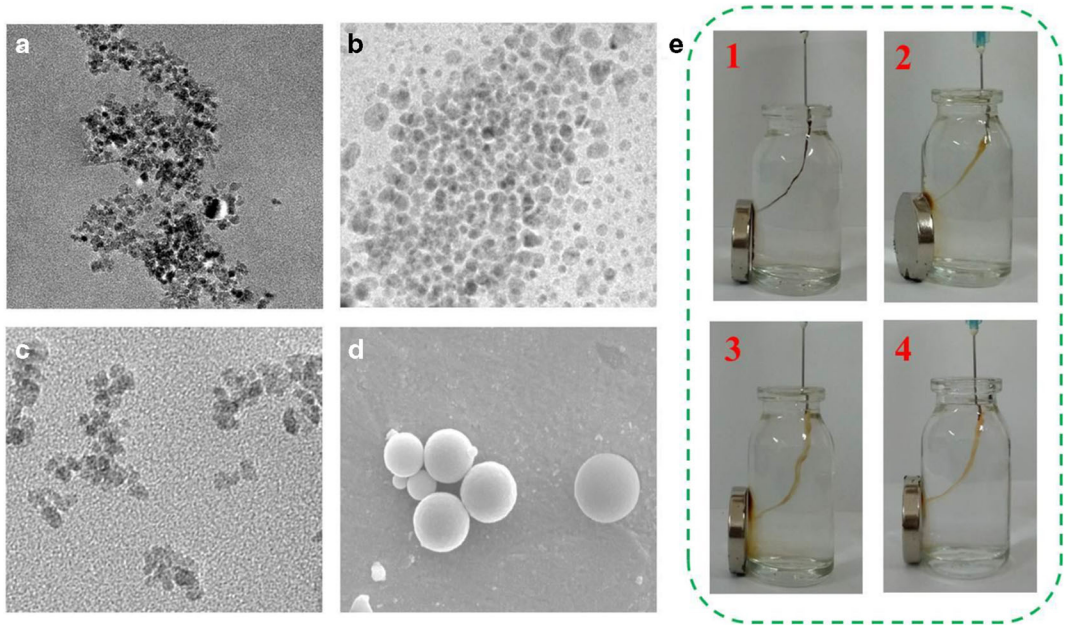

Fig. 1 TEM images of γ-Fe_2O_3 NPs (**a**), NP_{CMCS} (**b**), NP_{PLGA} (**c**), and SEM image of NP_{HSA} (**d**). The γ-Fe_2O_3 NPs, NP_{CMCS}, NP_{PLGA}, and NP_{HSA} response to an external magnetic field in DI water (**e**), and the magnetic-responsiveness numbered 1, 2, 3, and 4 was corresponding to γ-Fe_2O_3 NPs, NP_{CMCS}, NP_{PLGA}, and NP_{HSA}, respectively

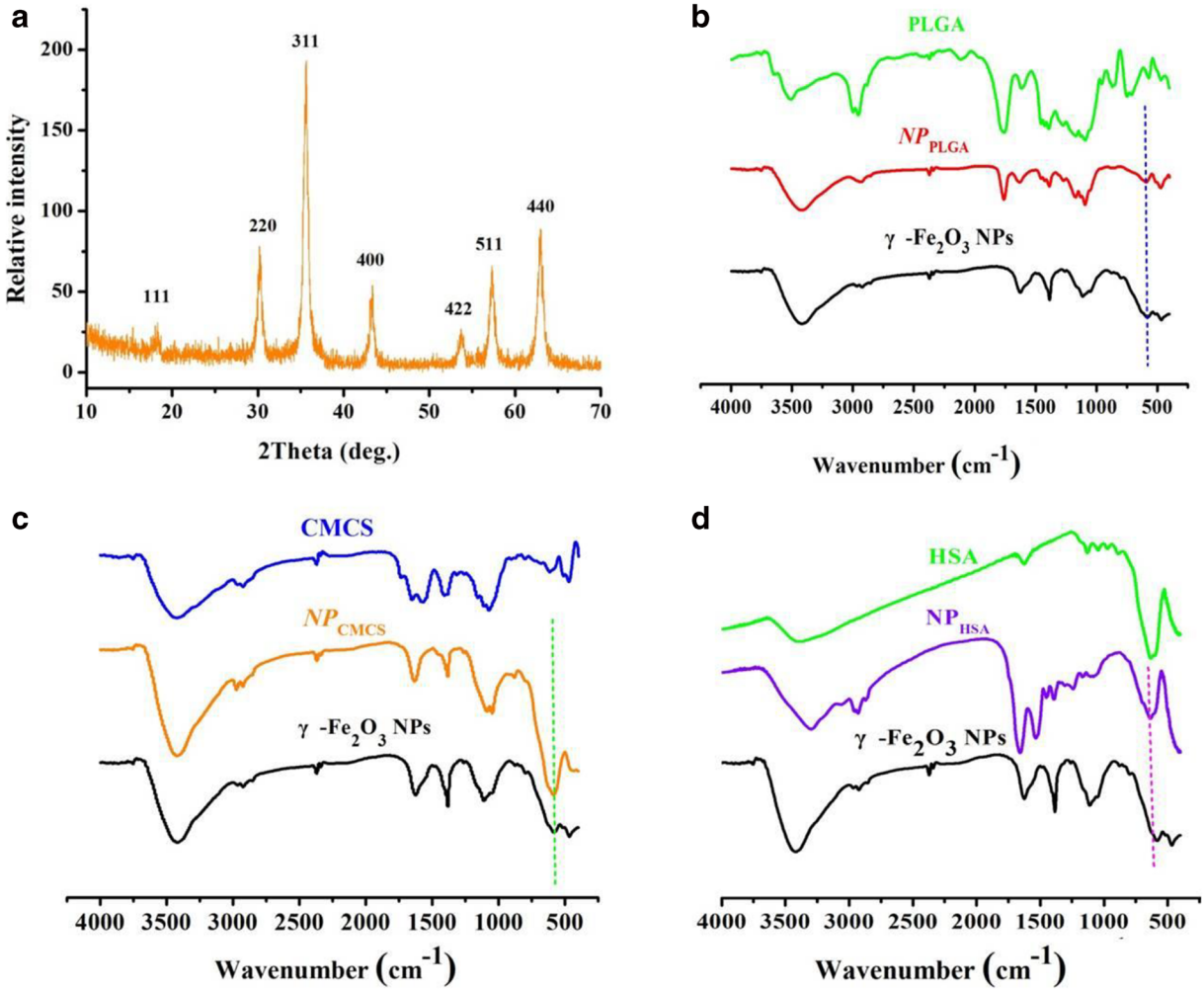

Fig. 2 XRD pattern of γ-Fe_2O_3 NPs (**a**). The FT-IR spectra of the γ-Fe_2O_3 NPs, NP_{PLGA} (**b**), NP_{CMCS} (**c**), and NP_{HSA} (**d**)

added into the above solution and then incubated at 37 °C for 10 min. (iii) The absorbance of the obtained solution was measured at 652 nm.

Total cholesterol detection in fetal bovine serum

Ten microliters of the diluted serum was incubated with 50 μL of cholesterol esterase (0.05 U/mL) for 15 min at 37 °C in the dark, and then, 40 μL PBS buffer solution was added up to 100 μL solution. The cholesterol detection was performed as mentioned above.

Image acquisition and analysis

Bright-field images were acquired using an inverted microscope (Eclipse TE 2000-U) equipped with a CCD camera (CV-S3200). Software Image-Pro Plus® 6.0 (Media Cyternetics) and SPSS 17.0 (SPSS Inc.) were used to perform image analysis and statistical data analysis, respectively. The quantitative data were presented as means ± standard deviation (SD) for each experiment. All experiments were performed with three replicates, and the results presented were from representative experiments.

Results and discussion

In the present work, we attempted to construct the layer-coating nanoparticles, i.e., NP_{PLGA}, NP_{CMCS}, and NP_{HSA}, and evaluate whether the surface modification would modulate the catalytic activity of γ-Fe_2O_3 NPs.

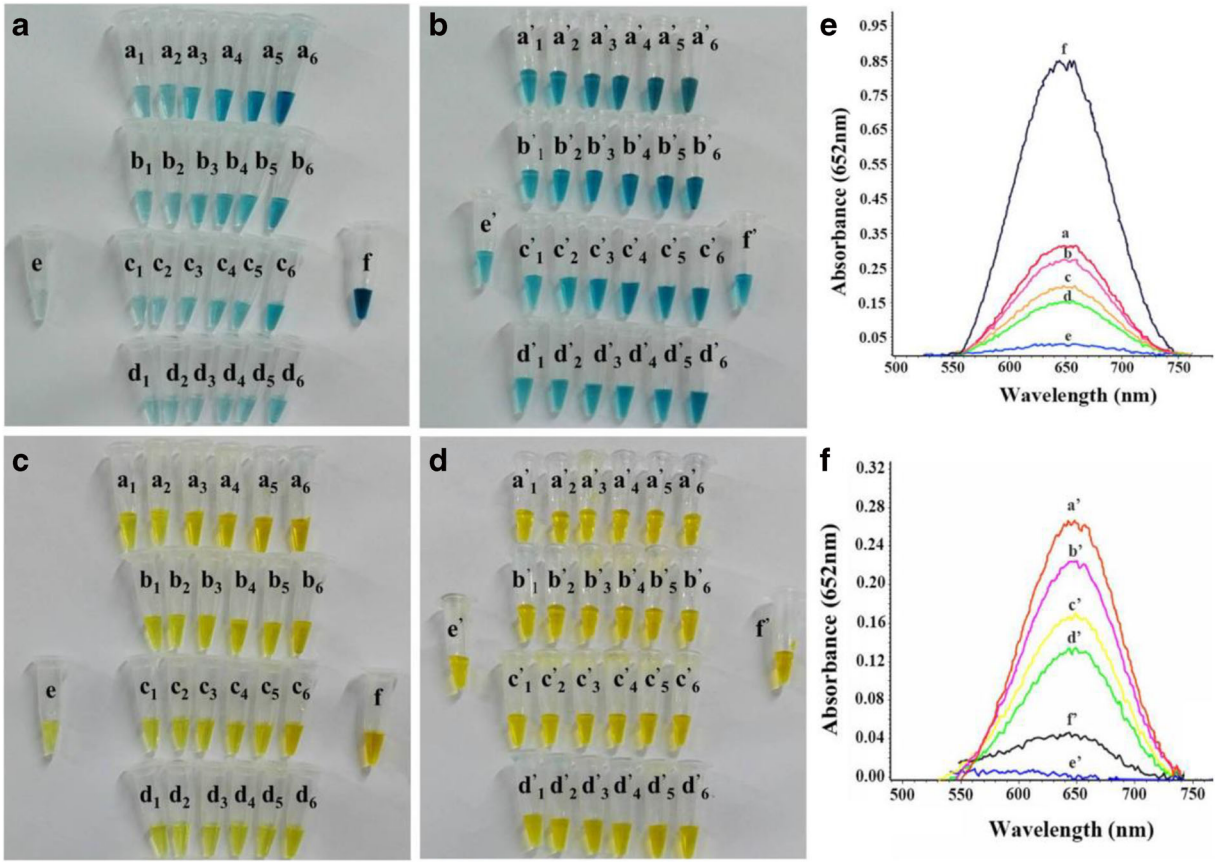

Fig. 3 **a** Peroxidase-like activity analysis of surface-modified magnetic nanoparticles, including γ-Fe_2O_3 NPs, NP_{PLGA}, NP_{CMCS}, and NP_{HSA} catalyze oxidation of peroxidase substrates TMB in the presence of H_2O_2 to produce blue-color reactions. Typical reactions are shown (a) γ-Fe_2O_3 + TMB + H_2O_2, (b) NP_{PLGA} + TMB + H_2O_2, (c) NP_{CMCS} + TMB + H_2O_2, (d) NP_{HSA} + TMB + H_2O_2, (e) negative control (H_2O_2 + TMB), (f) positive control (POD + TMB + H_2O_2), (a_1–a_6, b_1–b_6, c_1–c_6, d_1–d_6: 5, 10, 25, 50, 100, 200 μg/mL). **b** The peroxidase-like activity of γ-Fe_2O_3 NPs, NP_{PLGA}, NP_{CMCS}, and NP_{HSA} after 6 h (various reaction systems corresponding to **a**). **c**(a_1–f) and **d**(a_1'–f') stopped the reactions using H_2SO_4 (0.5 M), corresponding to (**a**, a_1-f) and (**b**, a_1'–f'), respectively. **e** Typical absorption spectra of TMB–H_2O_2. Reaction solutions catalytically oxidized by γ-Fe_2O_3 NPs (a_1-a_6), NP_{PLGA} (b_1-b_6), NP_{CMCS} (c_1-c_6), NP_{HSA} (d_6), negative control (e), positive control (f) in the presence of 12.8 μL H_2O_2 and 200 μg/mL various nanoparticles. **f** After 6 h reaction, UV-Vis spectrum of a′$_6$, b′$_6$, c′$_6$, d′$_6$, e′, and f′ correspond to a_6, b_6, c_6, d_6, e, and f

The detection mechanism is illustrated in Scheme 1 (Gao et al. 2017). With the catalysis activity of the prepared NP_{PLGA}, NP_{CMCS}, and NP_{HSA}, TMB was oxidized by H_2O_2 to form oxTMB showing an obvious blue color change in solutions. The absorbance of oxTMB at 652 nm was used to monitor the concentration of H_2O_2 (Josephy et al. 1982). Cholesterol used as a model analyte was under detection, since H_2O_2 is the oxidative product of cholesterol in the presence of ChOx; cholesterol can be indirectly detected.

The morphology and structure of γ-Fe_2O_3 NPs, NP_{PLGA}, NP_{CMCS}, and NP_{HSA} were characterized with the transmission electron microscope (TEM) and scanning electron microscope (SEM), Fourier-transform infrared spectrum (FT-IR), and X-ray diffractometer (XRD). As shown in Fig.1, the prepared γ-Fe_2O_3 NPs were morphologically uniform, and the diameter ranged from 10 to 15 nm (Fig. 1a), and the finalized NP_{CMCS} and NP_{PLGA} also displayed a mono-dispersed sphere with a uniform size of approximately 40–60 nm (Fig. 1b, c). Figure 1d shows the SEM image of the prepared NP_{HSA}, which indicated that the NP_{HSA} were uniform and round with an average diameter of 1 μm and well-distributed, even when dried. In addition, the analysis of the magnetic responsiveness of the prepared nanoparticles showed that the satisfactory magnetic-responsive properties were obtained in DI water with external magnetic fields (Fig. 1e).

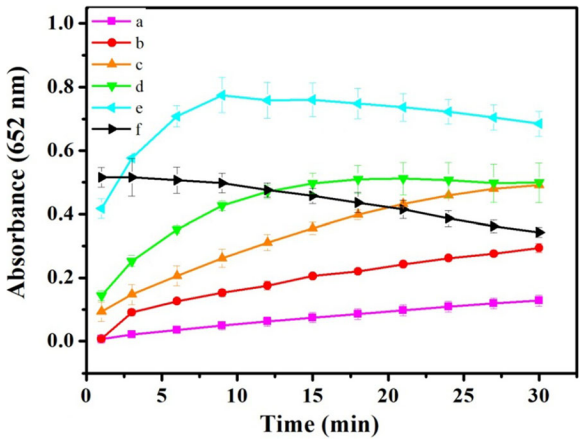

Fig. 4 Absorbance of TMB solution at different time points for different catalytic reactions: (a) negative control (H_2O_2 + TMB), (b) NP_{HSA} + TMB + H_2O_2, (c) NP_{CMCS} + TMB + H_2O_2, (d) NP_{PLGA} + TMB + H_2O_2, (e) γ-Fe_2O_3 + TMB + H_2O_2. (f) positive control (25 ng POD + TMB + H_2O_2). Reaction condition: 0.6 M H_2O_2, 100 μM TMB, 50 μg/mL γ-Fe_2O_3 NPs, NP_{PLGA}, NP_{CMCS}, and NP_{HSA} in 0.2 M NaAc buffer (pH 3.6), 37 °C

The X-ray powder diffraction (XRD) pattern of the prepared nanoparticles proved its crystalline nature, and their peaks matched well with standard γ-Fe_2O_3 reflections. Although the product was brown, yet the α-Fe_2O_3 phase was not observed (Fig. 2a). Figure 2b–d show the FT-IR spectra of the γ-Fe_2O_3 NPs, NP_{PLGA}, NP_{CMCS}, and NP_{HSA}; the results confirmed that the γ-Fe_2O_3 NPs were successfully coated by PLGA, CMCS, and HSA, in which the characteristic adsorption band of Fe–O was observed at 584 cm^{-1}, 586 cm^{-1}, and 616 cm^{-1} respectively.

The stability of the prepared NP_{PLGA}, NP_{CMCS}, and NP_{HSA} was assayed with transmittance in DI water at different time points. As presented in Fig. S1, the data indicated that the NP_{PLGA}, NP_{CMCS}, and NP_{HSA} could be uniformly dispersed and remained relatively stable in DI water.

The peroxidase-like activity of prepared γ-Fe_2O_3 NPs, NP_{PLGA}, NP_{CMCS}, and NP_{HSA} was evaluated by the catalytic oxidation of TMB in the presence of H_2O_2. Magnetite nanoparticles could catalyze the oxidation of the typical peroxidase substrates such as TMB in the presence of H_2O_2 to produce a blue color reaction with maximum absorbance at 652 nm. As shown in Fig. 3a, the prepared γ-Fe_2O_3 NPs, NP_{PLGA}, NP_{CMCS}, and NP_{HSA} produced a blue color in the presence of H_2O_2 and TMB, indicating that these nanoparticles have remarkable peroxidase-like activity and can catalyze the TMB oxidation. The enzymatic activity was further characterized by detecting the absorption peaks of oxTMB at 652 nm. The corresponding absorption spectra are shown in Fig. 3e, in which no absorption peak was recorded in negative control (TMB–H_2O_2) solution without a catalyst, while the other systems with different catalysts all had absorption peaks at 652 nm. Furthermore, the reaction time has certain effect on peroxidase-like activity. After 6 h, the blue color of the prepared γ-Fe_2O_3 NPs, NP_{PLGA}, NP_{CMCS}, and NP_{HSA} have

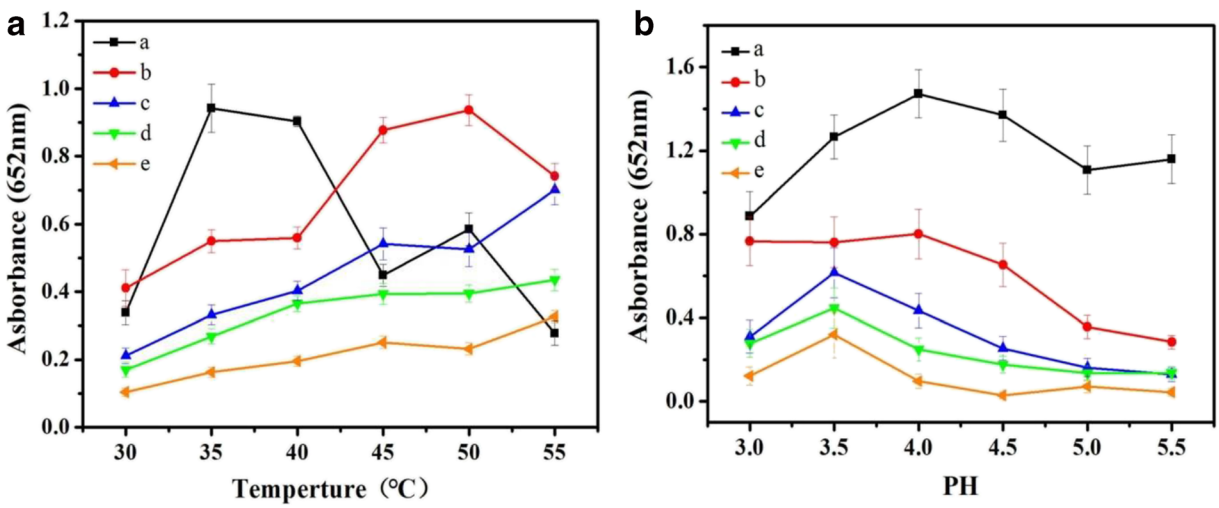

Fig. 5 Comparison of the stability of γ-Fe_2O_3 NPs, NP_{PLGA}, NP_{CMCS}, NP_{HSA}, and natural enzyme POD. Peroxidase activities were measured at 30–55 °C (**a**) or pH 3.0–5.5 (**b**) under standard conditions. **a** 25 ng POD +100 μM TMB + 0.6 M H_2O_2. **b** 50 μg/mL γ-Fe_2O_3 + 100 μM TMB + 0.6 M H_2O_2. **c** 50 μg/mL NP_{PLGA} + 100 μM TMB + 0.6 M H_2O_2. **d** 50 μg/mL NP_{CMCS} + 100 μM TMB + 0.6 M H_2O_2. **e** 50 μg/mL NP_{HSA} + 100 μM TMB + 0.6 M H_2O_2

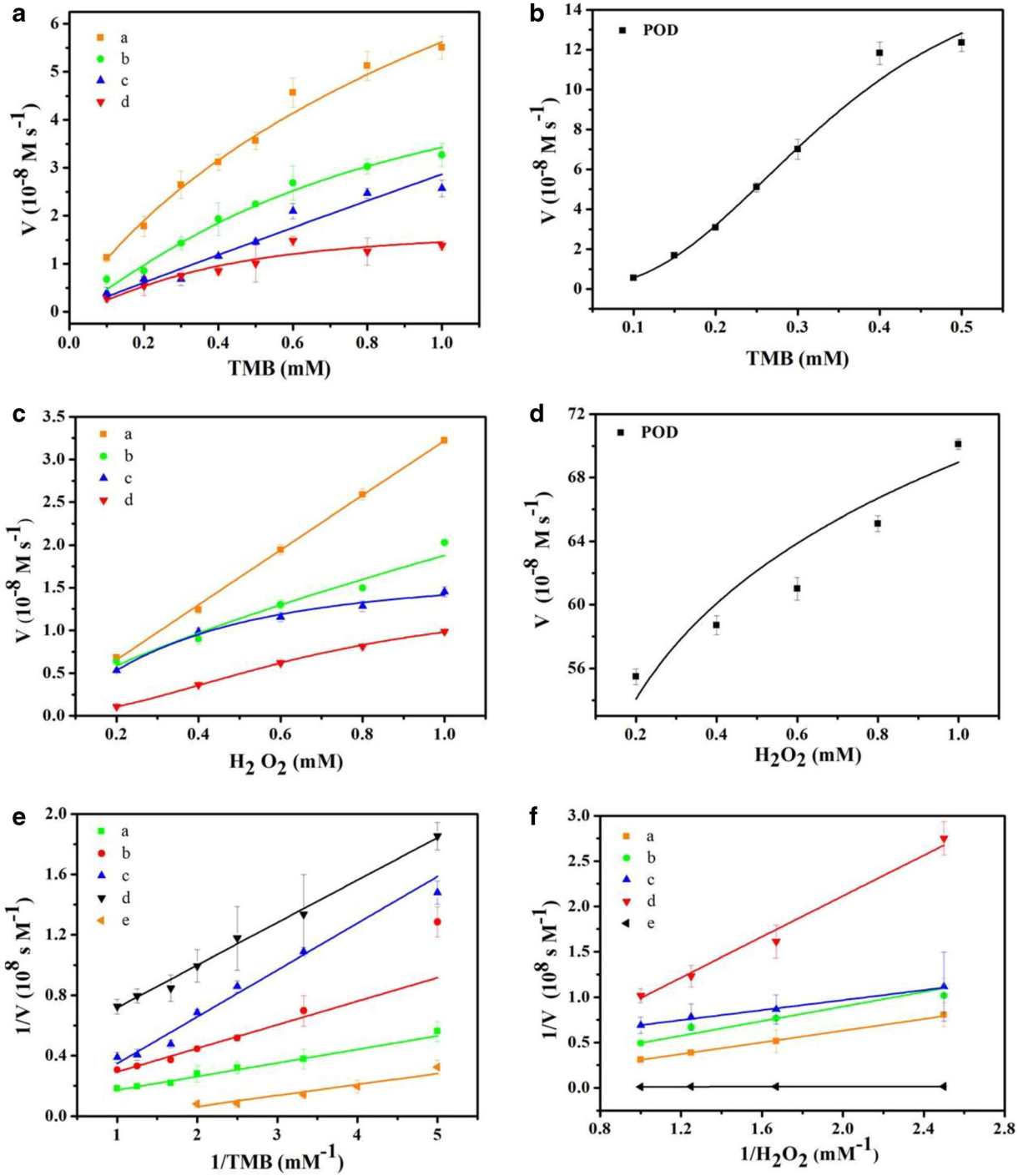

Fig. 6 Steady-state kinetic assays of prepared nanoparticles and POD as catalysts for the oxidation of TMB by H_2O_2.The initial reaction velocity (*V*) was measured under standard conditions. Kinetic assays toward TMB. Plot of *V*against TMB concentration, in which H_2O_2 concentration was fixed at 0.6 mM (**a**), and positive control POD (**b**). Kinetic assays toward H_2O_2 (**c**). Plot of *V*against H_2O_2 concentration, in which TMB concentration was fixed at 0.8 mM, and positive control POD (**d**). Double-reciprocal plot generated from **a** and **b** (**e**). Double-reciprocal plot generated from **c** and **d** (**f**). (a) γ-Fe_2O_3 NPs, (b) NP_{PLGA}, (c) NP_{CMCS}, (d) NP_{HSA}, (e) POD, respectively

Table 1 Comparison of the Michaelis–Menten (K_m) and maximum reaction velocity (V_{max})

Catalyst	Substrate	K_m (mM)	V_{max} (10^{-8} M s^{-1})
POD	TMB	1.98	40.68
	H_2O_2	0.30	113.70
γ-Fe_2O_3	TMB	1.24	13.01
	H_2O_2	21.54	66.71
NP_{PLGA}	TMB	0.90	6.61
	H_2O_2	4.41	10.93
NP_{CMCS}	TMB	3.63	12.60
	H_2O_2	0.66	2.40
NP_{HSA}	TMB	0.60	2.26
	H_2O_2	8.51	7.57

deepened, while the color in the positive control POD has changed from dark blue to light blue (Fig. 3b). The corresponding absorption spectra are shown in Fig. 3f in which the absorbance of POD dropped rapidly even closer to that of the negative control. Like enzymatic peroxidase activity, this color reaction was quenched by adding H_2SO_4 (Gao et al. 2007). As shown in Fig. 3 c and d, the reactions were stopped by adding 50 μL of 0.5 M H_2SO_4. All these results confirmed that the surface-modified NP_{PLGA}, NP_{CMCS}, and NP_{HSA} exhibited an intrinsic peroxidase-like activity.

Catalysis of natural enzymes or nanoenzymes was influenced by reaction time, temperature, and pH (Wei and Wang 2008). So the catalytic relative activity of the prepared NP_{PLGA}, NP_{CMCS}, and NP_{HSA} were

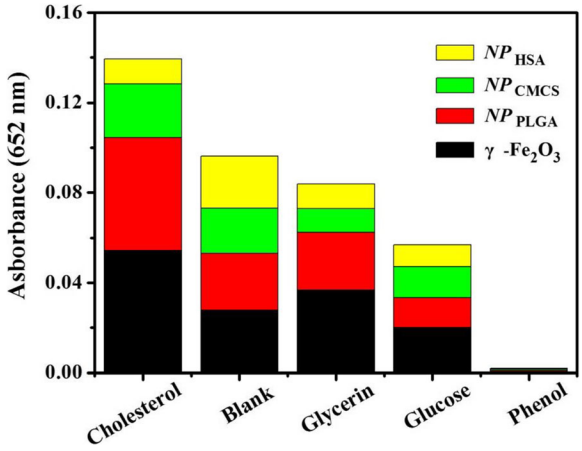

Fig. 7 Absorbance of the solutions with different substances for cholesterol detection. All measurements were performed in NaAc buffer solution (pH 3.6) containing 0.8 mM TMB at 37 °C. The concentration was 0.5 mM for cholesterol and 2 mM for the other interfering substances

investigated under varying reaction time (from 5 to 30 min), temperature (from 30 to 55 °C) and pH (from 3 to 5.5). The effects of reaction time on peroxidase-like activity of prepared NP_{PLGA}, NP_{CMCS}, and NP_{HSA} are shown in Fig. 4. The oxidation reaction was finished within 10–15 min, demonstrating a fast oxidation rate of TMB catalyzed by γ-Fe_2O_3 NPs, NP_{PLGA}, NP_{CMCS}, and NP_{HSA} in the presence of H_2O_2. The absorbance of the γ-Fe_2O_3 NPs–TMB–H_2O_2 system at 652 nm is much higher as compared with that of the other reaction systems. Nanoparticle enzyme activity gradually increased and finally stabilized within 30 min.

As shown in Fig. 5a, the activity of γ-Fe_2O_3 NPs, NP_{PLGA}, NP_{CMCS}, and NP_{HSA} was relatively stable and significantly higher than POD enzyme activity with temperature ranging from 40 to 55 °C, whereas the activity of POD dramatically decreased when the temperature exceeded 35 °C, implying that the catalytic activity of these surface-modified nanoparticles was less sensitive to temperature. In addition, the catalytic activity of NP_{PLGA}, NP_{CMCS}, and NP_{HSA} could still retain a capable catalytic activity even at 55 °C, but the catalytic activity of γ-Fe_2O_3 NPs decreased when the temperature was beyond 50 °C.

As shown in Fig. 5b, the catalytic activity of γ-Fe_2O_3 NPs, NP_{PLGA}, NP_{CMCS}, and NP_{HSA} was much higher between pH 3.0 and pH 3.5, which indicated that acidic buffer around with pH 3.5 might be an optimal condition to ensure a capable catalytic activity of these nanoparticles. Meanwhile, compared with natural enzyme POD, these fabricated nanoparticles also display a less sensitive response to pH change in a wider range.

To better understand the peroxidase-like catalytic activity of prepared γ-Fe_2O_3 NPs, NP_{PLGA}, NP_{CMCS}, and NP_{HSA}, the steady-state kinetic parameters for catalyzing TMB oxidation was analyzed with varying concentrations of TMB and H_2O_2 under the optimal condition. As illustrated in Fig. 6a–d, the initial catalytic velocity was followed with the typical Michaelis–Menten behaviors. Under the optimum conditions, a series of initial reaction rates were calculated and applied with the double reciprocal of the Michaelis −Menten equation (Fig. 6e, f) deduced from the Lineweaver−Burk plots (Dong et al. 2012).

The maximum initial velocity (V_{max}) and the Michaelis−Menten constant (K_m) were calculated by using the Lineweaver–Burk plots of double reciprocal of the Michaelis–Menten equation (Table 1). The V_{max} value is a direct measure of the enzymatic catalytic

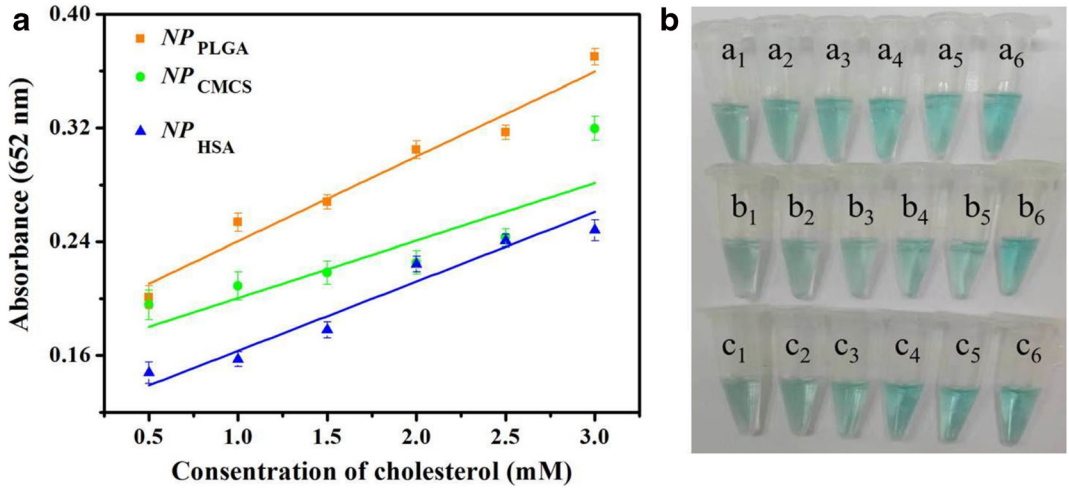

Fig. 8 **a** The standard curve for cholesterol detection and **b** the corresponding colored products NP_{PLGA} (a_1-a_6), NP_{CMCS} (b_1-b_6), NP_{HSA} (c_1-c_6)

activity. K_m is identified as an indicator of enzyme affinity to substrates. A low K_m represents a high affinity (Asati et al. 2009). The kinetic analysis showed that γ-Fe_2O_3 NPs ($K_m = 1.24$), NP_{PLGA} ($K_m = 0.9$), and NP_{HSA} ($K_m = 0.6$) demonstrated a higher affinity toward TMB than POD ($K_m = 1.98$) at acidic pH. However, NP_{CMCS} ($K_m = 3.63$) showed a lower affinity toward TMB than POD ($K_m = 1.98$). In addition, the calculation also showed that K_m value of γ-Fe_2O_3 NPs ($K_m = 21.54$), NP_{PLGA} ($K_m = 4.41$), NP_{CMCS} ($K_m = 0.66$), and NP_{HSA} ($K_m = 8.51$) for H_2O_2 was higher than POD ($K_m = 0.30$), suggesting that γ-Fe_2O_3, NP_{PLGA}, NP_{CMCS}, and NP_{HSA} require a higher concentration of H_2O_2 for depicting the same peroxidase activity as POD (Gao et al. 2007).

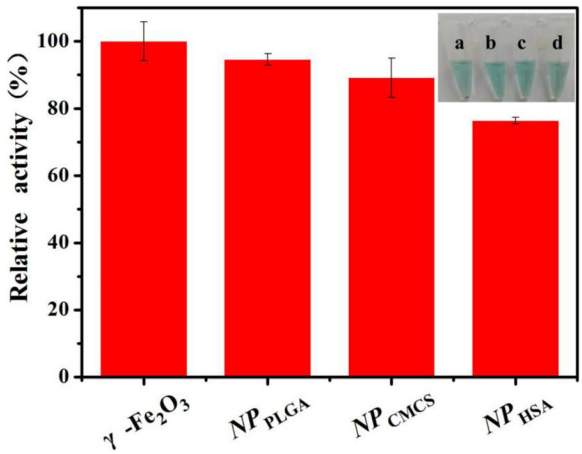

Fig. 9 Catalytic activity of prepared nanoparticles for cholesterol detection in fetal bovine serum. Inset: the colored products of (a) γ-Fe_2O_3 NPs, (b) NP_{PLGA}, (c) NP_{CMCS}, and (d) NP_{HSA}

Cholesterol could be oxidized by ChOx to produce H_2O_2 in the presence of oxygen (Shen and Liu 2007). The concentration of H_2O_2 monitored is indirectly related to the concentration of cholesterol. Therefore, the color change from the converted TMB could be used to measure the concentration of cholesterol. As shown in Fig. 7, a visualized detection of cholesterol can be catalyzed by the assembly of ChOx and the prepared nanoparticles, which provided a simple protocol for the determination of cholesterol.

To calculate the limit of detection (LOD) based on the standard $LOD = 3SD/S$, where SD is the standard deviation of the blank, and S is the slope of the sample and calibration curve. Therefore, we could calculate the LOD of NP_{PLGA}, NP_{CMCS}, and NP_{HSA} as 118 μM, 142 μM, and 96 μM, respectively. The possible interfering substances in blood samples were investigated, and as in Fig. 8, the results showed that the absorbance of these interfering substances was not evident when their concentrations are four times as high as that of cholesterol.

Furthermore, catalysis ability of these prepared nanoparticles was evaluated using cholesterol as a substrate in fetal bovine serum. As mentioned above, the total serum cholesterol generally included free cholesterol and cholesterol ester. Cholesterol esterase can effectively convert cholesterol ester to free cholesterol (Lu et al. 2015), and therefore, total cholesterol level was equivalent to free cholesterol level after the enzyme

hydrolysis of cholesterol ester. The free cholesterol response signals were detected readily as this bio-sensing approach was applied to serum samples (Zhang et al. 2017). As shown in Fig. 9, a blue solution was obtained in the serum, and the catalysis data showed that γ-Fe_2O_3 NPs and the modified nanoparticles can detect cholesterol in serum, and comparatively, the peroxidase-like activity of γ-Fe_2O_3 NPs was largely retained after the modification of HSA, PLGA, and CMCS.

Conclusions

In this work, we have synthesized the distinct layer-coating nanoparticles including NP_{PLGA}, NP_{CMCS}, and NP_{HSA}, and their peroxidase-like activity was explored with TMB as a substrate. The naked γ-Fe_2O_3 NPs exhibited a high intrinsic peroxidase-like activity, and the fabricated nanoparticles (NP_{PLGA}, NP_{CMCS}, and NP_{HSA}) were also followed with the classical Michaelis–Menten kinetics with much wider PH and temperature ranges, which could be effectively used for the visualized colorimetric cholesterol detection. In general, we believe these modified nanoparticles endowed with peroxidase-like activity may be widely used in various bioassays in the future.

Funding information This work was supported by the National Natural Science Foundation of China (No. 815 725 74, 314 008 55), the Scientific and Technological Project of Henan Province (No. 182 102 210 394), the Young Core Instructor Program in Higher Education Institution of Henan province (No. 2018 GGJS 067), and the Young Core Instructor Program from Henan University of Technology (No. 214 200 55).

Compliance with ethical standards

Conflict of interest The authors declare that they have no conflicts of interest.

References

Alexiou C, Arnold W, Klein JR, Parak GF, Hulin P, Bergemann C, Erhardt W, Wagenpfeil S, Lübbe SA (2000) Locoregional cancer treatment with magnetic drug targeting. Cancer Res 60:6641–6648

Asati A, Santra S, Kaittanis C, Nath S, Perez JM (2009) Oxidase-like activity of polymer-coated cerium oxide nanoparticles. Angew Chem Int Ed 48:2308–2312

Bertholon I, Hommel H, Labarre D, Vauthier C (2006) Properties of polysaccharides grafted on nanoparticles investigated by EPR. Langmuir 22:5485–5490

Boni A, Albertazzi L, Innocenti C, Gemmi M, Bifone A (2013) Water dispersal and functionalization of hydrophobic iron oxide nanoparticles with lipid-modified poly (amidoamine) dendrimers. Langmuir 29:10973–10979

Chen Z, Yin JJ, Zhou TY, Zhang Y, Song L, Song M, Hu S, Gu N (2012) Dual enzyme-like activities of iron oxide nanoparticles and their implication for diminishing cytotoxicity. ACS Nano 6:4001–4012

Chen Q, Wang X, Wang C, Feng L, Li Y, Liu Z (2015) Drug-induced self-assembly of modified albumins as nanotheranostics for tumor-targeted combination therapy. ACS Nano 9:5223–5233

Chen LK, Lin SY, Chen MJ, Wu HC, Jeng CC, Wang ML (2018) A sensitive platform for in vitro immunoassay based on biofunctionalized magnetic nanoparticles and magneto-optical faraday effect. Sensors Actuators B Chem 258:947–951

Chung HT, Hsiao KJ, Hsu CS, Yao M, Chen CY, Wang WS, Kuo PYM, Yang SC, Huang MD (2011) Iron oxide nanoparticle-induced epidermal growth factor receptor expression in human stem cells for tumor therapy. ACS Nano 5:9807–9816

Cormode PD, Gao L, Koo H (2017) Emerging biomedical applications of enzyme-like catalytic nanomaterials. Trends Biotechnol 36:15–29

Deda DK, Cardoso RM, Uchiyama MK, Pavani C, Toma SH, Baptista MS, Araki K (2017) A reliable protocol for colorimetric determination of iron oxide nanoparticle uptake by cells. Anal Bioanal Chem 409:6663–6675

Dong YL, Zhang HG, Rahman ZU, Su L, Chen XJ, Hu J, Chen XQ (2012) Graphene oxide-Fe_3O_4 magnetic nanocomposites with peroxidase-like activity for colorimetric detection of glucose. Nanoscale 4:3969–3976

Ebrahimisadr S, Aslibeiki B, Asadi R (2018) Magnetic hyperthermia properties of iron oxide nanoparticles: the effect of concentration. Physica C 549:119–121

Gao L, Zhuang J, Nie L, Zhang J, Zhang Y, Gu N, Wang T, Feng J, Yang D, Perrett S, Yan X (2007) Intrinsic peroxidase-like activity of ferromagnetic nanoparticles. Nat Nanotechnol 2:577–583

Gao L, Fan K, Yan X (2017) Iron oxide nanozyme: a multifunctional enzyme mimetic for biomedical applications. Theranostics 7:3207–3227

Guimaraes GPP, Gaglione S, Sewastianik T, Carrasco DR, Langer R, Mitchell JM (2018) Nanoparticles for immune cytokine TRAIL-based cancer therapy. ACS Nano 12:912–931

Gupta KA, Curtis GSA (2004) Lactoferrin and ceruloplasmin derivatized superparamagnetic iron oxide nanoparticles for targeting cell surface receptors. Biomaterials 25:3029–3040

Hasanzadeh M, Bahrami A, Alizadeh M, Shadjou N (2013) Magnetic nanoparticles loaded on mobile crystalline material-41: preparation, characterization and application as a novel material for the construction of an electrochemical nanosensor. RSC Adv 3:24237–24246

Hemalatha T, Prabu P, Gowthaman KM (2018) Fabrication and characterization of dual acting oleyl chitosan functionalised

iron oxide/gold hybrid nanoparticles for MRI and CT imaging. Int J Biol Macromol 112:250–257

Ishihara T, Maeda T, Sakamoto H, Takasaki N, Shigyo M, Ishida T, Kiwada H, Mizushima Y, Mizushima T (2010) Evasion of the accelerated blood clearance phenomenon by coating of nanoparticles with various hydrophilic polymers. Biomacromolecules 11:2700–2706

Josephy PD, Eling T, Mason RP (1982) The horseradish peroxidase-catalyzed oxidation of 3,5,3′,5′-tetramethylbenzidine free radical and charge-transfer complex intermediates. J Biol Chem 257:3669–3675

Kalidasan V, Liu X, Herng TS, Yang Y, Ding J (2016) Bovine serum albumin-conjugated ferrimagnetic iron oxide nanoparticles to enhance the biocompatibility and magnetic hyperthermia performance. Nano-Micro Lett 8:80–93

Kim B, Seo B, Park S, Lee C, Kim OJ, Oh TK, Lee SE, Choi GH, Youn SY (2017) Albumin nanoparticles with synergistic antitumor efficacy against metastatic lung cancers. Colloid Surface B 158:157–166

Kurczewska J, Cegłowski M, Schroeder G (2018) Preparation of multifunctional cascade iron oxide nanoparticles for drug delivery. Mater Chem Phys 211:34–41

Liang M, Fan K, Pan Y, Jiang H, Wang F, Yang D, Lu D, Feng J, Zhao J, Yang L, Yan X (2013) Fe_3O_4 magnetic nanoparticle peroxidase mimetic-based colorimetric assay for the rapid detection of organophosphorus pesticide and nerve agent. Anal Chem 85:308–312

Lin Y, Ren J, Qu X (2014) Catalytically active nanomaterials: a promising candidate for artificial enzymes. Acc Chem Res 47:1097–1105

Liu Y, Yu F (2011) Substrate-specific modifications on magnetic iron oxide nanoparticles as an artificial peroxidase for improving sensitivity in glucose detection. Nanotechnology 22: 145704

Lu C, Liu X, Li Y, Yu F, Tang L, Hu Y, Ying Y (2015) Multifunctional Janus hematite-silica nanoparticles: mimicking peroxidase-like activity and sensitive colorimetric detection of glucose. ACS Appl Mater Interfaces 7:15395–15402

Mahmoudi M, Simchi A, Imani M, Häfeli UO (2009) Superparamagnetic iron oxide nanoparticles with rigid cross-linked polyethylene glycol fumarate coating for application in imaging and drug delivery. J Phys Chem C 113: 8124–8131

Min C, Shao H, Liong M, Yoon JT, Weissleder R, Lee H (2012) Mechanism of magnetic relaxation switching sensing. ACS Nano 6:6821–6828

Olsvik O, Popovic T, Skjerve E, Cudjoe KS, Hornes E, Ugestad J, Uhlén M (1994) Magnetic separation techniques in diagnostic microbiology. Clin Microbiol Rev 7:43–54

Pérez RA, Albero B, Tadeo JL, Molero E, Sánchez-Brunete C (2015) Application of magnetic iron oxide nanoparticles for the analysis of PCBs in water and soil leachates by gas chromatography–tandem mass spectrometry. Anal Bioanal Chem 407:1913–1924

Peterson DR, Chen W, Cunningham TB, Andrade EJ (2015) Enhanced sandwich immunoassay using antibody-functionalized magnetic iron-oxide nanoparticles for extraction and detection of soluble transferrin receptor on a photonic crystal biosensor. Biosens Bioelectron 74:815–822

Qu S, Yang H, Ren D, Kan S, Zou G, Li D, Li M (1999) Magnetite nanoparticles prepared by precipitation from partially reduced ferric chloride aqueous solutions. J Colloid Interface Sci 215:190–192

Shen J, Liu CC (2007) Development of a screen-printed cholesterol biosensor: comparing the performance of gold and platinum as the working electrode material and fabrication using a self-assembly approach. Sensors Actuators B Chem 120:417–425

Singh S (2016) Cerium oxide based nanozymes: redox phenomenon at biointerfaces. Biointerphases 11:04B202

Situ FC, Samia CA (2014) Highly efficient antibacterial iron oxide@carbon nanochains from wustite precursor nanoparticles. ACS Appl Mater Interfaces 6:20154–20163

Soares PIP, Laia TAC, Carvalho A, Pereira JCL, Coutinho TJ, Ferreira MMI, Novo MMC, Borges PJ (2016) Iron oxide nanoparticles stabilized with a bilayer of oleic acid for magnetic hyperthermia and MRI applications. Appl Surf Sci 383:240–247

Sun YK, Ma M, Zhang Y, Gu N (2004) Synthesis of nanometer-size maghemite particles from magnetite. Colloids Surf A Physicochem Eng Asp 245:15–19

Vallabani NV, Karakoti AS, Singh S (2017) ATP-mediated intrinsic peroxidase-like activity of Fe_3O_4-based nanozyme: one step detection of blood glucose at physiological pH. Colloid Surface B 153:52–60

Varshosaz J, Soheili M (2008) Production and in vitro characterization of lisinopril-loaded nanoparticles for the treatment of restenosis in stented coronary arteries. J Microencapsul 25: 478–486

Wan Q, Jiang R, Guo L, Yu S, Liu M, Tian J, Liu G, Deng F, Zhang X, Wei Y (2017) Novel strategy toward AIE-active fluorescent polymeric nanoparticles from polysaccharides: preparation and cell imaging. ACS Sustain Chem Eng 5:9955–9964

Wang J, Wang X, Ren L, Wang Q, Li L, Liu W, Wan Z, Yang L, Sun P, Ren L, Li M, Wu H, Wang J, Zhang L (2009) Conjugation of biomolecules with magnetic protein microspheres for the assay of early biomarkers associated with acute myocardial infarction. Anal Chem 81:6210–6217

Wang X, Cao W, Qin L, Lin T, Chen W, Lin S, Yao J, Zhao X, Zhou M, Hang C, Wei H (2017) Boosting the peroxidase-like activity of nanostructured nickel by inducing its 3+ oxidation state in $LaNiO_3$ perovskite and its application for biomedical assays. Theranostics 7:2277–2286

Wang D, Ding W, Zhou K, Guo S, Zhang Q, Haddleton MD (2018) Coating titania nanoparticles with epoxy-containing catechol polymers via cu (0)-LRP as intelligent enzyme carriers. Biomacromolecules 19:2979–2990

Wei H, Wang E (2008) Fe_3O_4 magnetic nanoparticles as peroxidase mimetics and their applications in H_2O_2 and glucose detection. Anal Chem 80:2250–2254

Yang CY, Wang TY, Tseng LW (2017) Amplified peroxidase-like activity in iron oxide nanoparticles using adenosine monophosphate: application to urinary protein sensing. ACS Appl Mater Interfaces 9:10069–10077

Zhang Y, Wang YN, Sun XT, Chen L, Xu ZR (2017) Boron nitride nanosheet/CuS nanocomposites as mimetic peroxidase for sensitive colorimetric detection of cholesterol. Sensors Actuators B Chem 246:118–126

Zhao T, Chen H, Dong Y, Zhang J, Huang H, Zhu J, Zhang W (2013) Paclitaxel- loaded poly (glycolide-co-ε-caprolactone)-b-D-α-tocopheryl polyethylene glycol 2000 succinate nanoparticles for lung cancer therapy. Int J Nanomedicine 8:1947–1957

Zhu L, Zhou Z, Mao H, Yang L (2017) Magnetic nanoparticles for precision oncology: theranostic magnetic iron oxide nanoparticles for image-guided and targeted cancer therapy. Nanomedicine (London) 12:73–87